Available online at www.sciencedirect.com
SCIENCE DIRECT®

Journal of the European Ceramic Society 24 (2004) 2095–2102

www.elsevier.com/locate/jeurceramsoc

Effect of composition and annealing temperature on the mechanical properties of a vitrified waste

P. Kavouras, Ph. Komninou*, Th. Karakostas

Physics Department, Aristotle University, 541 24 Thessaloniki, Greece

Received 26 February 2003; accepted 25 May 2003

Abstract

The microhardness and indentation fracture toughness of a vitrified industrial waste, in the form of ash, were characterized by the method of static indentation test. These properties were investigated as a function of composition and thermal treatment conditions. To further understand the influence of the constitutive oxides, additional measurements were made in a series of synthetic products, where a mixture of iron and lead oxides was used as a substitute for the ash. The underlying deformation mechanisms controlling the mechanical properties of such complex systems as determined by static indentation tests are discussed. It was found that plasticity, in the amorphous products, is mainly governed from the silica content, even in the cases where silica is not found in sufficient quantity in order to build an extended three-dimensional vitreous network. On the other hand, the morphology of the separated crystalline phases is the dominant factor affecting plasticity in the glass-ceramic products.

Keywords: Fracture; Glass; Glass ceramics; Hardness; Vitrified waste; Waste materials

1. Introduction

The combustion of industrial solid wastes is a common practice to obtain solid residues with considerably reduced residual toxicity, as a result of the decomposition of the majority of the toxic organic compounds. Oxide glasses and glass–ceramics with complex compositions can be obtained from the stabilization of such toxic residues with the vitrification method.[1–3] The vitrified products can comprise potentially marketable materials appropriate for construction or decorative purposes.[4,5]

A significant number of studies dedicated to the interpretation of mechanical properties of oxide glasses have been published.[6–8] These studies have gathered knowledge concerning the effective indentation energy absorbing mechanisms, i.e. deformation mechanisms that determine the hardness of a vitreous material. Additionally, a limited number of studies have been dedicated to the investigation of the relative importance of the deformation mechanisms as a function of temperature.[9–11] A universal behavior of the hardness of oxide glasses is still lacking, and as a result, the mechanical properties of glassy materials with more complex compositions, as those obtained from the vitrification of solid wastes, are still rather obscure and need to be carefully investigated.

In the present study, the microhardness and indentation fracture toughness (IFT) of the SiO_2–Na_2O–ash vitrified system was elaborated as a function of the ash content and consequent thermal treatment conditions by the static indentation test (SIT) method. This investigation was made since the appropriate mechanical properties and chemical stability constitute the necessary conditions for the commercialization of such materials. The ash is the solid residue originating from the combustion of a rich in tetraethyl lead waste that is found as sediment in the bottom of leaded gasoline tanks in sludge form. Vitrification was achieved with silica (SiO_2) powder that was added to the batch composition and hematite (Fe_2O_3) that is a component of the ash. These oxides were combined together for the construction of an extended three-dimensional vitreous network with efficient structural integrity.[12] Additionally,

* Corresponding author. Tel.: +30-2310-99-81-95; fax: +30-2310-99-80-61.
E-mail address: komnhnoy@auth.gr (P. Komninou).

0955-2219/03/$ - see front matter © 2003 Elsevier Ltd. All rights reserved.
doi:10.1016/S0955-2219(03)00356-X

soda ash (Na_2O) was used as a melting agent since it is a network modifier similar to lead oxide (PbO), which is a solid waste component and has a similar structural behavior. Thus, the vitrified products have a complex composition, consisting of two glass formers and two glass modifiers. Consequently, their mechanical behavior cannot be deduced from the existing literature. The study is further complicated from the potential reduction of hematite to magnetite (Fe_3O_4) during batch melting,[13,14] since these iron oxides have opposing structural role.[15,16]

The morphology and microstructure of all as-quenched and thermally treated samples were analysed by scanning electron microscopy (SEM) and analytical transmission electron microscopy (TEM), using imagine, electron diffraction analysis and energy dispersive spectroscopy. The morphology of the devitrified products depends on the initial matrix composition and on the thermal treatment conditions. As a result, the mechanical properties of the devitrified products, especially IFT, are compared with the as-vitrified ones in a more critical manner, since the comparison is made between a vitreous-single phase and a vitroceramic-multiphase material.[17]

The influence of each of the constituent oxides on the mechanical properties of the vitrified samples is understood from the investigation of the synthetic vitrified samples, i.e. the oxide glass system SiO_2–Na_2O–PbO–Fe_2O_3, where a mixture of iron and lead oxides is the substitute for the solid waste. This can be proved a useful oxide glass model system for the investigation of the physical properties of vitrified waste products, originating from oil distillery facilities, since the relative amount of PbO and Fe_2O_3 may vary significantly.

2. Experimental

All vitrified samples were prepared by conventional batch melting in a Pt crucible at 1400 °C for 2 h and subsequent rapid cooling on a stainless steel plate at ambient atmosphere. All ash containing as-quenched products were thermally treated at 900 °C in order to induce crystal phase separation. This temperature was found to be sufficiently high for the completion of the devitrification process, as it was verified by differential thermal analysis (DTA). In the case of W60 product an additional annealing treatment at 720 °C was required, since it has been shown that the devitrification process in this composition is a two-step process.[18] Thermal treatment was composed of a heating stage with a constant rate of 10 °C/min followed by an isothermal step of 30 min. The sample was then slowly cooled down at room temperature. The density of all samples was measured by the Archimedes method.[19]

All batch compositions together with the composition of the ash and the density values of the corresponding vitrified products are listed in Table 1. Compositions W40–W60 were synthesized, in order to stabilize the ash content. The above products can sufficiently captivate the polluting agents of the ash, by rendering the lead content non-leachable.[12] The W(s)40–W(s)60 are the respective synthetic products, where the ash has been replaced by a mixture of iron (Fe_2O_3) and lead oxides (PbO). The relative weight proportion of these oxides was chosen to be 3/2 in order to obtain a Fe/Pb atomic ratio comparable with that of the ash. These products were synthesized in order to resolve whether the microhardness and IFT values of the W40–W60 products could be simulated by adding the two aforementioned metallic oxides instead of the ash. Products S1–S3 were synthesized with the same relative weight proportion of iron and lead oxide as the synthetic products so as to obtain vitreous products with Si/O atomic ratio in the vicinity of 0.33. According to oxide glass formation, 0.33 is the lowest Si/O value that an extended three-dimensional vitreous network can be formed.[20,21] By scanning this compositional region, it can be deduced if the passage through Si/O = 0.33 leads to an abrupt change of the mechanical properties.

All vitreous and devitrified products were sliced by a diamond wheel and mechanically polished by SiC grinding papers and Al_2O_3 pastes. The microhardness was measured by an Anton Paar MHT-10 microhardness tester attached on a Zeiss Axiolab-A metallographic microscope by which all optical micrographs were also obtained. For each sample the Indentation Size Effect (ISE)[22,23] curve was constructed in the load region of 0.05–1.5 N. This analysis was made in order to resolve the load at which all indentation measurements would be performed; this load should lie in the plateau region of the ISE curves, i.e. in the region where the microhardness value is independent of the size of the indentation. The plateau region starts in all samples at 0.5–0.6 N, and all measurements were made applying 0.8 N with the lowest loading rate obtainable from the microhardness tester used (0.2 N/s). In this way, the microhardness values (H_K) can be safely compared

Table 1
Batch compositions prepared for the vitrification process (wt.%)

Ash	Fe_2O_3	PbO	SiO_2	Na_2O	Density (g/cm^3)	Vitrified product
40	–	–	50	10	2.90	W40
50	–	–	35	15	3.19	W50
60	–	–	25	15	3.40	W60
–	24	16	50	10	3.14	W(s)40
–	30	20	35	15	3.42	W(s)50
–	36	24	25	15	3.68	W(s)60
–	18	12	49	21	2.97	S1
–	22.8	15.2	43.4	18.6	3.10	S2
–	33	22	31.5	13.5	3.46	S3

Ash composition (wt.%): 47.3 Fe_2O_3, 37.4 $PbOPbBr_2$, 2.3 $PbSO_4$, 2.0 PbO, 2.2 SiO_2, 1.5 Al_2O_3, 3.3 other oxides, 4.0 humidity.

between different samples. A number of 12 indentations were performed to obtain each microhardness value at room temperature with a Knoop diamond indenter. In the case of the thermally treated glass–ceramic products the Knoop indentations were made on the residual vitreous matrix in order to exclude plastic deformation phenomena associated with the separated crystallites.

The indentation fracture toughness (K_{IC}) was obtained by measuring the length of the median crack system produced on the surface of the samples from the indentation of a Vickers diamond indenter applying the equation:[24,25]

$$K_{IC} = \delta(E/H_K)^{1/2}\left(P/c^{3/2}\right), \quad (1)$$

where E is the elastic modulus, P the indentation load, c the crack length and δ a constant with a value of 0.016 for a Vickers indenter geometry. The above measurements were made by obtaining 20 indentations that produced isotropic microcrack propagation, i.e. the microcracks emanate from all four corners of the indentation print as shown in Fig. 1. The elastic modulus was calculated from the equation:[26]

$$d/D = 1/7.11\text{-}0.45(H_K/E), \quad (2)$$

where d and D are the smaller and longer diagonals of a Knoop indentation print, respectively.

3. Results

The microhardness and IFT values of the as-vitrified products together with the corresponding Si/O atomic ratio are listed in Table 2. In the first six samples the microhardness and IFT values decrease with decreasing silica content or with decreasing Si/O atomic ratio, as it is depicted in Fig. 2. The same behaviour was observed for the S1–S3 samples as shown in Fig. 3. The microhardness values of the vitrified ash products and the respective synthetic products are the same within the experimental errors, as it is listed in Table 2. From this

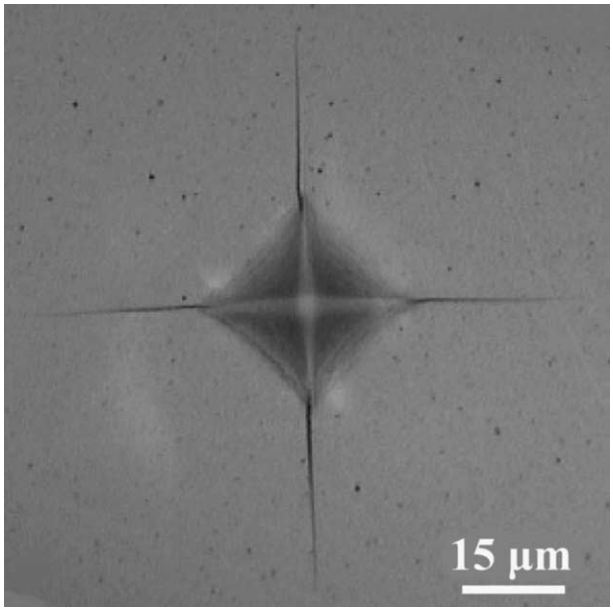

Fig. 1. A characteristic Vickers indentation with isotropic microcrack propagation pattern. Such indentation prints were used to measure IFT.

Table 2
The microhardness and IFT values, with the corresponding experimental errors, are presented together with the Si/O atomic ratio of the vitrified products

Vitrified product	Si/O (atomic ratio)	H_K (GPa)	K_{IC} (MPa m$^{1/2}$)
W40	0.37	4.1±0.05	0.57±0.02
W50	0.30	3.9±0.05	0.53±0.02
W60	0.25	3.8±0.05	0.51±0.02
W(s)40	0.36	4.0±0.05	0.58±0.02
W(s)50	0.28	3.8±0.05	0.54±0.02
W(s)60	0.22	3.7±0.05	0.53±0.02
S1	0.35	4.3±0.05	0.58±0.02
S2	0.32	4.1±0.05	0.57±0.01
S3	0.27	3.7±0.05	0.54±0.02

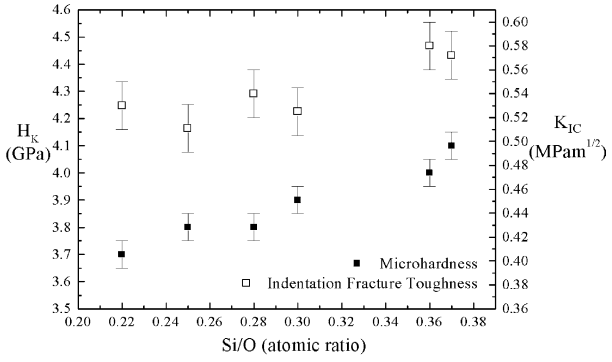

Fig. 2. Microhardness and IFT values of the vitrified ash-containing products and their corresponding synthetic products as a function of the Si/O atomic ratio.

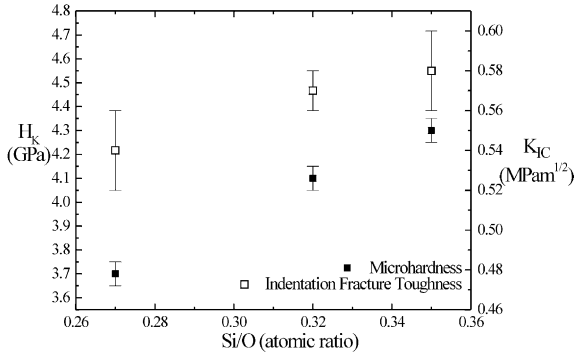

Fig. 3. Microhardness value and IFT of the synthetic products S1–S3 as a function of the Si/O atomic ratio.

it can be concluded that the replacement of the ash with a mixture of Fe_2O_3 and PbO did not affect appreciably the susceptibility to plastic deformation (microhardness) and the resistance to crack propagation (fracture toughness).

The mechanical properties of the thermally treated ash-containing vitrified products are listed in Table 3. Thermal treatment at 900 °C of W(1)40 product did not produce detectable devitrification in the scale of transmission electron microscopy resolution.[27] In this case, the microhardness value was not affected, while IFT was increased. Thermal treatment of W(1)50 product at 900 °C, caused microhardness value increase and a decrease in the IFT value, while devitrification occurred with the growth of crystallites of tetragonal morphology, belonging to the $Pb_8Fe_2O_{11}$ phase.[27]

W(1)60 and W(2)60 products were found to have a different morphology due to the separation of different crystalline phases (Table 3) and as a result the mechanical properties were modified. Hexagonal crystalline flakes of Magnetoplumbite ($PbFe_{12}O_{19}$) were homogeneously dispersed in W(1)60 product; the microhardness value increased, while the IFT value decreased with respect to the as-quenched W60 product. Magnetoplumbite crystallites and extended crystalline foils of Hematite (Fe_2O_3) were separated in W(2)60 product.[18] In this case both microhardness and IFT values were increased. Thermal treatment leads to an increase in the density value only in the cases where devitrification occurs. This is due to the higher density of the separated crystalline phases with respect to the vitreous matrix of the as-quenched products.

4. Discussion

4.1. Microhardness

In order to interpret the results of microhardness all possible plastic deformation mechanisms that absorb indentation energy in an amorphous material should be considered. It has been reported[7,28] that these mechanisms are: (a) plastic (viscous) flow due to shear, (b) densification resulting from compression and shear which in some cases may invoke breaking of bonds, and (c) fracture. Since, all Knoop indentations used for microhardness measurements were crackles,[29] fracture can be excluded from the following analysis of microhardness results. According to the above, the size of an indentation print depends on the susceptibility of plastic flow and densification to absorb the energy imposed from the indenter. In the case that these mechanisms can easily absorb energy, the size of an indentation print will be larger, therefore the calculated microhardness value will be lower.

A relatively lower Si/O ratio represents a less cross-linked vitreous network (a network with relatively fewer Si–O–Si bonds or more non-bridging oxygens), i.e. a softer glass structure.[30] Consequently, plastic flow and densification produced from shear stress during the indentation process, is more difficult to occur in a more cross-linked network,[31–33] since plastic deformation requires the rupture of a larger number of atomic bonds. Thus, according to these two mechanisms, the experimental results of microhardness value are in agreement with the above analysis. In Fig. 4, characteristic optical

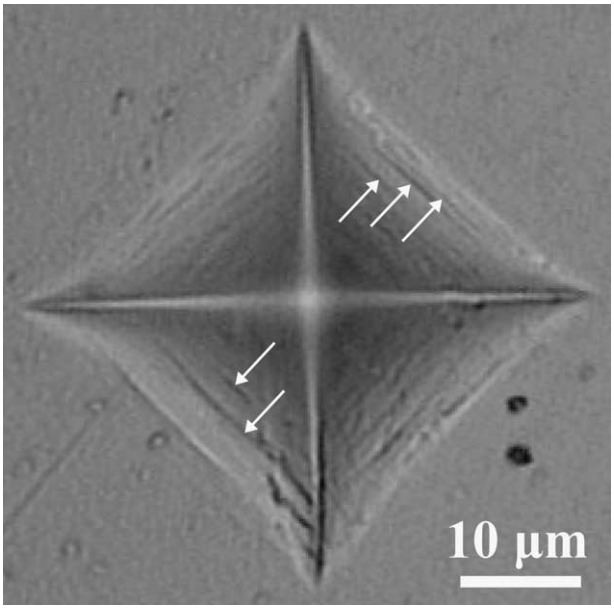

Fig. 4. An optical micrograph of a Vickers indentation print on a polished section of the W40 product. The white arrows denote some of the shear bands, which are indicative of plastic flow normal to their trace.

Table 3
Effect of the thermal process conditions on the microhardness and IFT values of the vitrified products that contain ash

Devitrified product	Annealing temperature (°C)	Density (g/cm^3)	Morphology	Separated phases	H_K (GPa)	K_{IC} (MPa m$^{1/2}$)
W(1)40	900	2.91	Vitreous	–	4.1±0.05	0.64±0.02
W(1)50	900	3.29	Vitroceramic	$Pb_8Fe_2O_{11}$	4.2±0.05	0.47±0.01
W(1)60	720	3.63	Vitroceramic	$PbFe_{12}O_{19}$	4.2±0.05	0.40±0.03
W(2)60	900	3.86	Vitroceramic	$PbFe_{12}O_{19} + Fe_2O_3$	4.2±0.05	0.62±0.03

micrograph of a Vickers indentation print on the surface of W40 product reveals a number of shear bands, indicating that plastic flow is active during indentation in the under study vitreous system.

TEM observations have shown that crystal phase separation is induced due to thermal treatment in W50 and W60 compositions.[18,27] In this way they become glass–ceramic composite materials with a hardened vitreous matrix that contains crystal phases of iron and mixed lead–iron oxides (Table 3). This suggests that the non-shearable homogeneously distributed crystallites increase the threshold for the onset of plastic flow. On the contrary, thermal treatment of W40 composition did not induce devitrification and microhardness value is virtually unaffected. This suggests that temperature treatment did not affect the onset of yielding in the average sense.

4.2. Indentation fracture toughness

IFT follows an analogous behavior to microhardness as a function of Si/O atomic ratio for all as-vitrified samples. A higher IFT value represents a reduced tendency for crack propagation designated by the length of the microcracks emanating from the corners of a Vickers indentation print. The propagation of a microcrack requires the rupture of atomic bonds. Therefore, a more interconnected vitreous network (higher Si/O ratio) is less susceptible to fracture since a microcrack of the same length would require rupture of a larger number of atomic bonds.

The IFT value of the annealed W(1)40 sample is considerably increased with respect to that of the as-vitrified one. This sample did not show any tendency to crystallize. The increase of the IFT value is associated to residual stress reduction that took place during thermal treatment.[34] The residual stresses are produced from the differential contraction in the centre and in the outer region of the samples. In such cases the crack growth is driven by the combined influence of residual stress and applied stress from the indentation.[35,36] Thus, thermal treatment reduced or eliminated one of the two driving forces for crack propagation. A characteristic optical micrograph of a Vickers indentation print from W(1)40 product is presented in Fig. 5a.

It has been reported though that in some cases annealing can cause a decrease in the fracture toughness of glasses.[37,38] This apparent discrepancy is on account of the fact that the above results have been obtained by the Chevron-Notch technique that is influenced from the surface residual compressive stress[38] responsible for thermal tempering, while the results of the present work were obtained from the interior of the samples.

Conversely, the IFT value of the W(1)50 and W(1)60 is reduced. The morphology and the size of the separated crystal phases is similar in the two above samples, with crystallites of a few micrometers homogeneously dispersed in their volume as it is visible in the optical micrographs shown in Fig. 5b and c. The two samples have been devitrified and though their microhardness value has been increased, the microcrack propagation occurs more easily. Fig. 5b and c depict two characteristic optical micrographs of Vickers indentation prints obtained from W(1)50 and W(1)60 samples, respectively. In this case, the critical stress required for crack propagation decreases as a result of the reduction of the effective surface energy due to the presence of amorphous/crystalline interfaces with poor adhesion. This results to a crack propagation pattern similar to intergranular fracture that reduces the IFT value.

Annealing of the W(2)60 product at 900 °C resulted to a glass–ceramic material with increased IFT value. The separated crystallites are able to annihilate microcrack propagation, as it is shown in the optical micrograph of Fig. 5d. In this highly anisotropic microcrack propagation pattern, the oblong hematite crystallites act as a barrier to microcrack propagation. The extended crystalline foils resist cracking propagation in the same way as in plastic flow and consequently, fracture separation phenomena, i.e. decohesion, between the crystalline and amorphous phases are not dominant.

All as-quenched synthetic samples were also thermally treated and their microhardness and IFT values were analogous with those obtained from the respective ash-containing ones. However, due to the inhomogeneity of the thermally treated products, the quantitative comparison of their values will not provide explicit conclusions. The qualitative similarity of the results can be shown by comparing Figs. 5d and e. Fig. 5e depicts a Vickers indentation print on W(s)60 product that was thermally treated at 900 °C. In both micrographs the oblong crystallites, indicated with white arrows, annihilate crack propagation.

4.3. General comments

The fact that the microhardness and IFT value is affected from the silica content is an indication that the mechanical properties of the system under study are mainly controlled by the degree of interconnection of the silica network. It seems that silica is the dominant glass former, even in the cases where it cannot construct an extended vitreous network. This is supported from the results obtained from the S2–S3 samples, where the Si/O atomic ratio is smaller than 0.33.

Since the microhardness and IFT values of the W40–W60 vitrified ash products are the same with the corresponding synthetic ones, within the experimental errors, it can be concluded that ash components, out of Fe_2O_3 and PbO, do not have a significant role in the determination of the mechanical properties. In this way,

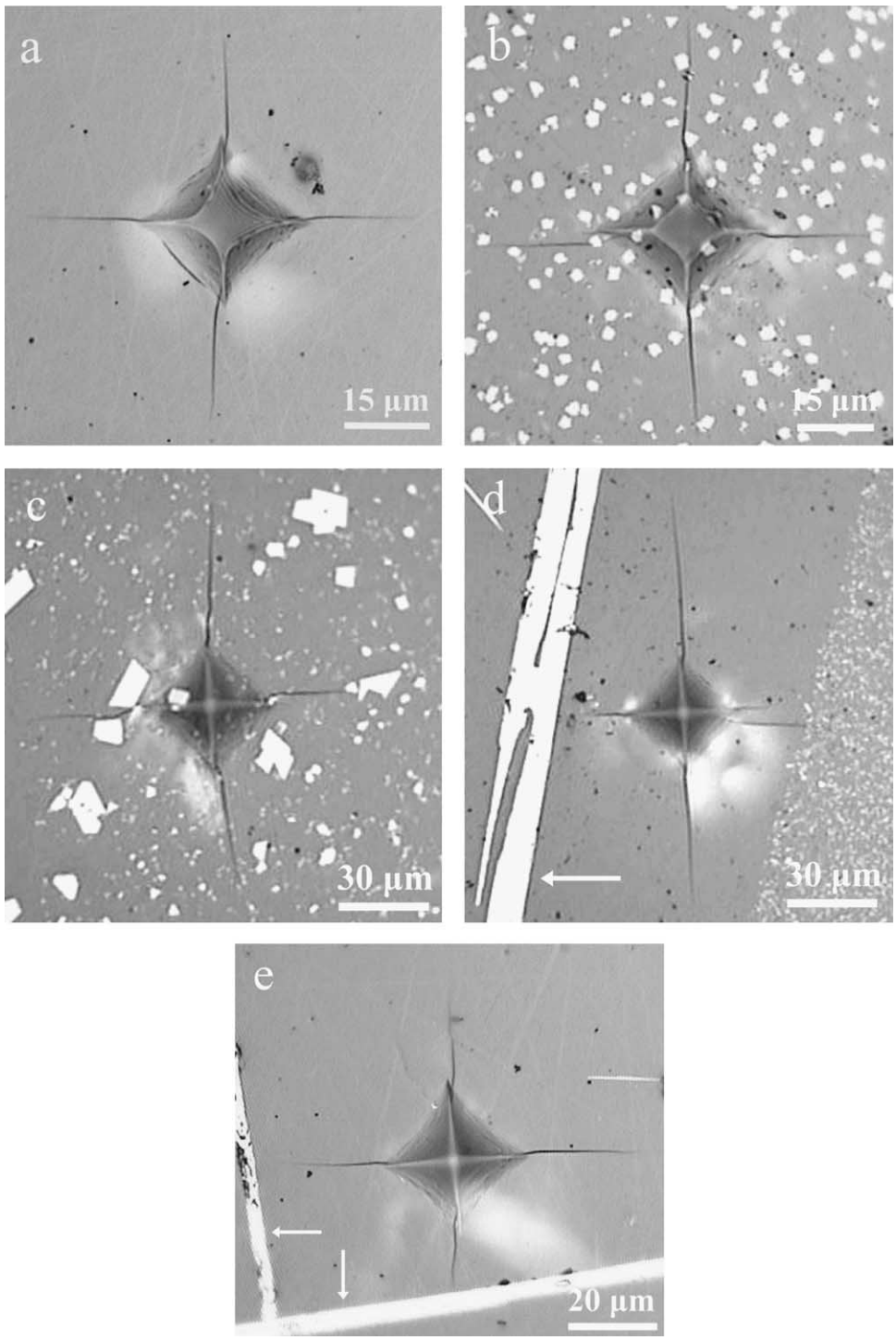

Fig. 5. Optical micrographs showing Vickers indentation prints performed on: (a) W(1)40, (b) W(1)50, (c) W(1)60, (d) W(2)60, and (e) W(s)60 thermally treated at 900 °C products. Crack propagation patterns in (b) and (c) micrographs are indicative of intergranular fracture. In (d) and (e) micrographs the oblong crystallites, indicated with white arrows, act as a barrier to microcrack propagation.

the mechanical properties of the specific vitrified waste products can be safely estimated by vitrifying a Fe_2O_3 and PbO powders mixture that simulates the ash-component of the vitrified waste products. This can be proved a useful result, for two main reasons: firstly, because the mechanical properties can be investigated by vitrifying significantly less hazardous materials and secondly, because the mechanical properties of vitrified wastes with different relative proportions of Fe_2O_3 and PbO can be estimated.

5. Conclusions

The plasticity in the vitreous system under study is mainly governed from the ability of silica to form an extended three-dimensional vitreous network. The above was proposed from the fact that the microhardness increases with increasing Si/O atomic ratio in all as-vitrified products. The relative increase of the microhardness value was interpreted by the increasing difficulty of densification and plastic flow to occur in a more cross-linked, i.e. cohesive, vitreous network. The indentation fracture toughness of the as-vitrified products followed the behavior of microhardness. This observation was interpreted using similar arguments: crack propagation requires breaking of a higher number of bonds in a more cross-linked vitreous network. The microhardness value of the residual matrix of the thermally treated samples was virtually constant when phase separation did not occur, while it increased in the devitrified products. The IFT value of the thermally treated products, compared to the as-vitrified, was highly depended on the susceptibility to crystal phase separation and on the separated crystallites morphology. Finally, both microhardness and IFT values of the vitrified waste products were the same, within the experimental errors, compared with their corresponding synthetic ones. Microhardness and fracture toughness values of the ash-containing as-quenched and thermally treated products are appropriate for their use for structural applications.

Acknowledgements

The authors would like to thank Professor Elias Aifantis for critical reading of the manuscript and fruitful discussions.

References

1. LaGrega, M. D., Buckingham, P. L. and Evans, J. C., *Hazardous Waste Management*. McGraw-Hill, New York, 2001.
2. Nazaroff, W. W. and Alvarez-Cohen, L., *Environmental Engineering Science*. John Wiley & Sons, 2001.
3. Corbitt, R. A., *Standard Handbook of Environmental Engineering*. McGraw Hill, New York, 1999.
4. Erol, M., Genç, A., Öveçodlu, M. L., Yücelen, E., Küçükbayrak, S. and Tapic, Y., Characterization of a glass-ceramic produced from thermal power plant fly ashes. *J. Europ. Cer. Soc.*, 2000, **20**, 2209–2214.
5. Erol, M., Küçükbayrak, S. O., Ersoy-Meriçboyu, A. and Öveçodlu, M. L., Crystallization behaviour of glasses produced from fly ashes. *J. Europ. Cer. Soc.*, 2001, **21**, 2835–2841.
6. Angell, C. A., Relaxation in liquids, polymers and plastic crystals—strong/fragile patterns and problems. *J. Non-Cryst. Solids*, 1991, **131-133**, 13–31.
7. Salama, S. N. and El-Batal, H. A., Microhardness of phosphate glasses. *J. Non-Cryst. Solids*, 1994, **168**, 179–185.
8. Sehgal, J. and Ito, S., Brittleness of glass. *J. Non-Cryst. Solids*, 1999, **253**, 126–132.
9. Le Bourhis, E. and Metayer, D., Indentation of glass as a function of temperature. *J. Non-Cryst. Solids*, 2000, **272**, 34–38.
10. Rouxel, T. and Sanglebœf, J. C., The brittle to ductile transition in a soda–lime–silica glass. *J. Non-Cryst. Solids*, 2000, **271**, 224–235.
11. Watanabe, T., Benino, Y. and Komatsu, T., Change in Vickers hardness at the glass transition region for fragile and strong glasses. *J. Non-Cryst. Solids*, 2001, **286**, 141–145.
12. Kavouras, P., Kaimakamis, G., Ioannidis, Th. A., Kehagias, Th., Komninou, Ph., Kokkou, S., Pavlidou, E., Antonopoulos, J., Sofoniou, M., Zouboulis, A., Hadjiantoniou, C. P., Prakouras, A. and Karakostas, Th., Vitrification of lead-rich solid ashes from incineration of hazardous industrial wastes. *Waste Manag.*, 2003, **23**, 361–371.
13. Karamanov, A., Pisciella, P. and Pelino, M., The crystallization kinetics of iron rich glass in different atmospheres. *J. Europ. Cer. Soc.*, 2000, **20**, 2233–2237.
14. Karamanov, A., Taglieri, G. and Pelino, M., Iron-rich sintered glass-ceramics from industrial wastes. *J. Am. Ceram. Soc.*, 1999, **82**, 3012–3016.
15. Wang, P. W. and Zhang, L., Structural role of lead in lead silicate glasses derived from XPS spectra. *J. Non-Cryst. Solids*, 1996, **194**, 129–134.
16. Mekki, A., Holland, D., McConville, C. F. and Salim, M., An XPS study of iron sodium silicate glass surfaces. *J. Non-Cryst. Solids*, 1996, **208**, 267–276.
17. Unyi, T., Juhász, A., Tasnádi, P. and Lendvai, J., Changes of the mechanical properties during the crystallization of bio-active glass–ceramics. *J. Mater. Sci.*, 2000, **35**, 3059–3068.
18. Kavouras, P., Komninou, Ph., Chrissafis, K., Kaimakamis, G., Kokkou, S., Paraskevopoulos, K. and Karakostas, Th., Microstructural changes of processed vitrified solid waste products. *J. Europ. Ceram. Soc.*, 2003, **23**, 1305–1311.
19. Anderson, B. W. and Jobbins, E. A., *Gem Testing*, 10th edn. Butterworths & Co., London, 1990.
20. Shelby, J. E., *Introduction to Glass Science and Technology*. RSC Paperbacks, Cambridge, 1997.
21. Pisciella, P., Crisucci, S., Karamanov, A. and Pelino, M., Chemical durability of glasses obtained by vitrification of industrial wastes. *Waste Manag*, 2001, **21**, 1–9.
22. Farges, G. and Degout, D., Interpretation of the indentation size effect in Vickers microhardness measurements—absolute hardness of materials. *Thin Solid Films*, 1989, **181**, 365–374.
23. Bull, S. J., Page, T. F. and Yoffe, E. H., An explanation of the indentation size effect in ceramics. *Phil. Mag. Let*, 1989, **59**, 281–288.
24. Antsis, G. R., Chantikul, P., Lawn, B. R. and Marshall, D. B., A critical evaluation of indentation techniques for determining fracture toughness: I, direct crack measurements. *J. Am. Ceram. Soc.*, 1981, **64**, 533–538.
25. Amin, K. A. In *Engineered Materials Handbook: Ceramics and Glasses*, ed. S. J. Schneider Jr. ASM International, 2000, pp. 599–601.
26. Marshall, D. B., Noma, T. and Evans, A. G., A simple method for determining elastic-modulus-to-hardness ratios using Knoop indentation measurements. *J. Am. Ceram. Soc.*, 1982, **65**, C175–C176.
27. Kavouras, P., Powder Processing for the Fabrication of Composite Materials for Technological Applications. PhD thesis, Aristotle University, Thessaloniki, 2003.
28. Doremus, R. H., *Glass Science and Technology*. John Wiley and Sons, New York, 1994.
29. Li, H. and Bradt, R. C., The effect of indentation-induced cracking on the apparent microhardness. *J. Mater. Sci.*, 1996, **31**, 1065–1070.
30. Rajendran, V., Nishara Begum, A., Azooz, M. A. and El-Batal,

F. H., Microstructural dependence of relevant physical–mechanical properties on SiO_2–Na_2O–CaO–P_2O_5 biological glasses. *Biomaterials*, 2002, **23**, 4263–4275.
31. Watanabe, T., Muratsubaki, K., Benino, Y., Saitoh, H. and Komatsu, T., Hardness and elastic properties of Bi_2O_3-based glasses. *J. Mater. Sci.*, 2001, **36**, 2427–2433.
32. Zhang, Z., Soga, N. and Hirao, K., Indentation deformation and fracture toughness of densified silicate glass. *J. Mater. Sci.*, 1995, **30**, 6359–6362.
33. Hirao, K., Yoshimoto, M., Soga, N. and Tanaka, K., Densification of magnesium and calsium metaphosphate glasses. *J. Non-Cryst. Sol*, 1991, **130**, 78–84.
34. Roach, D. H. and Cooper, A. R., Effect of contact residual stress relaxation on fracture strength of indented soda–lime glass. *J. Am. Ceram. Soc.*, 1985, **68**, 632–636.
35. Marshall, D. B. and Lawn, B. R., Flaw characteristics in dynamic fatigue: the influence of residual contact stresses. *J. Am. Ceram. Soc.*, 1980, **63**, 532–536.
36. Fuller, E. R., Lawn, B. R. and Cook, R. F., Theory of fatigue for brittle flaws originating from residual stress concentrations. *J. Am. Ceram. Soc.*, 1983, **66**, 314–321.
37. Reddy, K. P. R., Fontana, E. H. and Helfinstine, J. D., Fracture toughness measurement of glass and ceramic materials using chevron-notched specimens. *J. Am. Ceram. Soc.*, 1988, **71**, C310–C313.
38. Boccaccini, A. R., Rawlings, R. D. and Dlouhý, I., Reliability of the chevron-notch technique for fracture toughness determination in glass. *Mater. Sci. Eng. A. Struct.*, 2003, **347**, 102–108.